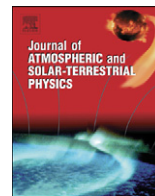




Contents lists available at ScienceDirect

# Journal of Atmospheric and Solar-Terrestrial Physics

journal homepage: [www.elsevier.com/locate/jastp](http://www.elsevier.com/locate/jastp)

## Responses of polar mesospheric cloud brightness to stratospheric gravity waves at the South Pole and Rothera, Antarctica

Xinzhao Chu<sup>a,\*</sup>, Chihoko Yamashita<sup>a</sup>, Patrick J. Espy<sup>b</sup>, Graeme J. Nott<sup>c</sup>,  
Eric J. Jensen<sup>d</sup>, Han-Li Liu<sup>e</sup>, Wentao Huang<sup>a</sup>, Jeffrey P. Thayer<sup>a</sup>

<sup>a</sup> Cooperative Institute for Research in Environmental Sciences and Department of Aerospace Engineering Sciences, University of Colorado at Boulder, USA

<sup>b</sup> Department of Physics, Norwegian University of Science and Technology, Trondheim, Norway

<sup>c</sup> Department of Physics and Atmospheric Science, Dalhousie University, Halifax, Canada

<sup>d</sup> NASA Ames Research Center, Moffett Field, CA, USA

<sup>e</sup> National Center for Atmospheric Research, Boulder, CO, USA

### ARTICLE INFO

#### Article history:

Accepted 7 October 2008

Available online 17 October 2008

#### Keywords:

Polar mesospheric clouds

Gravity waves

Lidar

Antarctica

Stratosphere

### ABSTRACT

We present the first observational proof that polar mesospheric cloud (PMC) brightness responds to stratospheric gravity waves (GWs) differently at different latitudes by analyzing the Fe Boltzmann lidar data collected from the South Pole and Rothera (67.5°S, 68.0°W), Antarctica. Stratospheric GW strength is characterized by the root-mean-square (RMS) relative density perturbation in the 30–45 km region and PMC brightness is represented by the total backscatter coefficient (TBC) in austral summer from November to February. The linear correlation coefficient (LCC) between GW strength and PMC brightness is found to be +0.09 with a 42% confidence level at the South Pole and –0.49 with a 98% confidence level at Rothera. If a PMC case potentially affected by a space shuttle exhaust plume is removed from the Rothera dataset, the negative correlation coefficient and confidence level increase to –0.61 and 99%, respectively. The Rothera negative correlation increases when shorter-period waves are included while no change is observed in the South Pole correlation. Therefore, observations show statistically that Rothera PMC brightness is negatively correlated with the stratospheric GW strength but no significant correlation exists at the South Pole. A positive correlation of +0.74 with a confidence level of 99.98% is found within a distinct subset of the South Pole data but the rest of the dataset exhibits a random distribution, possibly indicating different populations of ice particles at the South Pole. Our data show that these two locations have similar GW strength and spectrum in the 30–45 km region during summer. The different responses of PMC brightness to GW perturbations are likely caused by the latitudinal differences in background temperatures in the ice crystal growth region between the PMC altitude and the mesopause. At Rothera, where temperatures in this region are relatively warm and supersaturations are not as large, GW-induced temperature perturbations can drive subsaturation in the warm phase. Thus, GWs can destroy growing ice crystals or limit their growth, leading to negative correlation at Rothera. Because the South Pole temperatures in the mesopause region are much colder, GW-perturbed temperature may never be above the frost point and have less of an impact on crystal growth and PMC brightness. The observed phenomena and proposed mechanisms above need to be understood and verified through future modeling of GW effects on PMC microphysics and ray modeling of GW propagation over the South Pole and Rothera.

© 2008 Elsevier Ltd. All rights reserved.

### 1. Introduction

Due to the water ice nature of polar mesospheric clouds (PMCs) (Hervig et al., 2001), PMCs are expected to be very sensitive to the changes in mesospheric water vapor and temperature (Thomas, 1991). The increased concentration of CH<sub>4</sub>, which oxidizes to form water vapor in the mesopause region

\* Corresponding author. Tel.: +1 303 492 3280; fax: +1 303 492 1149.  
E-mail address: Xinzhao.Chu@Colorado.edu (X. Chu).

(Thomas et al., 1989), and CO<sub>2</sub>, which possibly cools the middle and upper atmosphere (Portman et al., 1995), could lead to the increase of PMC brightness and occurrence frequency (Thomas, 1996; Thomas and Olivero, 2001). Thus, PMCs provide a potential indicator of global climate change, which has fueled the intensive study of PMCs in recent years. While earlier trend studies concentrated on PMC occurrence frequency (Gadsden, 1998; DeLand et al., 2003), recent studies turn the attention to PMC brightness (DeLand et al., 2007). Two major considerations are behind this change. First, unlike the occurrence frequency that is heavily affected by sampling issues, PMC brightness is a

better-defined physical quantity readily measured by satellites and lidars. Second, occurrence frequency might reach saturation, especially at high latitudes where it is nearly 100% in midsummer. Conversely, PMC brightness could continue growing with larger number density and/or larger PMC ice particles. Therefore, PMC brightness is more suitable for long-term trend monitoring. However, PMC brightness is strongly influenced by tides (von Zahn et al., 1998; Chu et al., 2001b, 2003, 2006; Fiedler et al., 2005), planetary waves (Merkel et al., 2003), and gravity waves (GWs) (Hecht et al., 1997; Gerrard et al., 1998, 2004a, b). To derive reliable long-term trends and to understand the meaning of these trends, it is important to understand and quantify PMC brightness response to various dynamic factors in addition to the basic water vapor, temperature, and nucleation parameters. This will help to validate and improve coupled PMC microphysical, chemical, and dynamical models so that long-term trends can be assessed based on these models and historic data sets.

The focus of this paper is the PMC brightness response to atmospheric GWs. The visual displays of PMCs, i.e., ground-viewed noctilucent clouds (NLCs), often exhibit GW signatures like bands, streaks, billows, and whirls (e.g., Witt, 1962; Gadsden and Schröder, 1989). When such wave-like NLC structures move through the lidar field of view, they are observed as variations of PMC brightness with time. It has been suggested that GWs cause PMC brightness to vary through wave-induced undulation of cloud layers and wave-induced convergence and divergence of cloud particle concentration (Jensen and Thomas, 1994), through wave breaking (Fritts et al., 1993), or through wave-induced temperature perturbations in the PMC vicinity (Turco et al., 1982; Jensen and Thomas, 1994; Rapp et al., 2002). Observations from Sondrestrom, Greenland (67.0°N, 50.9°W) showed evidence of the passage of acoustic GWs in the mesopause region causing PMC sublimation (Hecht et al., 1997). Gerrard et al. (1998, 2004a, b) analyzed the Rayleigh lidar data from Sondrestrom and found that the strength of stratospheric GWs (30–45 km) was negatively correlated with the PMC brightness. Furthermore, Thayer et al. (2003) employed a PMC microphysical model and found that the introduction of short period waves (2–3 h) replicated the cloud characteristics observed by the Rayleigh lidar at Sondrestrom.

None of the above investigations of GW and PMC correlations were conducted at very high latitude (i.e., not close to the pole). Whether this negative GW–PMC correlation is true for all latitudes becomes a valid question considering the latitudinal differences in background temperatures. Will GWs affect PMC microphysics in different ways under different background conditions? To answer these questions, we examine the extensive data collected by an iron Boltzmann lidar at Rothera (67.5°S, 68.0°W) and the South Pole (90°S) and derive the correlation between stratospheric GWs (30–45 km) and PMC using a statistical approach similar to Gerrard et al. (1998, 2004a). As Rothera is located at the edge of Antarctica and the South Pole at the center of the Antarctic plateau, the lidar datasets provide a unique opportunity to test a hypothesis that a negative correlation exists at the Antarctic edge but no correlation exists at the South Pole. Furthermore, by applying different temporal filters to select different period waves, we examine how this GW–PMC correlation varies with GW spectrum. We then investigate why the PMC brightness responds to GWs differently at different latitudes.

## 2. Methodology

### 2.1. Instrument

The instrument used to collect the observational data was the University of Illinois Fe Boltzmann/Rayleigh/Mie lidar. This is a

zenith-pointing lidar with dual channels operating at 372 and 374 nm. A detailed description of the lidar operation principles, system configurations, and measurement capabilities can be found in Chu et al. (2002). Due to its short operating wavelengths, high power, and daytime capability, this lidar is highly sensitive in detecting aerosols and clouds in the mesosphere (~85 km), even under the full sunlit conditions at the South Pole and Rothera (Chu et al., 2001a, b, 2003, 2004, 2006). Above the lower atmosphere aerosol layers (>30 km) and below the Fe layers (<70 km), this lidar is used as a powerful Rayleigh scattering lidar. Thus, the atmospheric density perturbations caused by GWs can be detected by the lidar and used to infer GW spectrum and strength in this region, as pioneered by several groups (e.g., Chanin and Hauchecorne, 1981; Gardner et al., 1989; Wilson et al., 1991a, b; Senft and Gardner, 1991; Gerrard et al., 1998).

### 2.2. Lidar data analysis for PMC and GWs

PMCs, shown as enhanced narrow scattering layers in lidar profiles, occur between 81 and 88 km at the South Pole and Rothera, with the cloud mean altitude at the South Pole (85.0 km) being 1 km higher than at Rothera (Chu et al., 2003, 2006). These lidar data have been analyzed for PMC studies at the South Pole by Chu et al. (2001a, b, 2003) and at Rothera by Chu et al. (2004, 2006). The cloud brightness in the current study is expressed as the total backscatter coefficient (TBC) measured by the Fe Boltzmann lidar and taken from Chu et al. (2003, 2006). The exact definition of TBC can be found in the Appendix A of Chu et al. (2003). TBC is the integration of PMC volume backscatter coefficient (VBC) through the entire PMC layer, equivalent to the cloud albedo measured by satellites. Therefore, TBC gives a better representation of the entire cloud brightness, compared to the peak VBC that only captures the layer peak brightness.

The analysis approaches for GW strength and spectrum are adapted from Gardner et al. (1989), Hostetler and Gardner (1990), Senft and Gardner (1991), and Gerrard et al. (1998, 2004a). Key points that are closely related to this paper are summarized below. The stratospheric GWs are characterized by the atmospheric relative density perturbations  $r(z, t)$  in the 30–45 km range defined as

$$r(z, t) \equiv \frac{\rho'(z, t)}{\rho_o(z, t)} \equiv \frac{\rho(z, t) - \rho_o(z, t)}{\rho_o(z, t)} \\ = \frac{\rho(z, t)/\rho(z_R, t) - \rho_o(z, t)/\rho(z_R, t)}{\rho_o(z, t)/\rho(z_R, t)} \quad (1)$$

where  $\rho_o(z, t)$  is the background atmospheric density,  $\rho(z, t)$  is the perturbed atmospheric density,  $\rho'(z, t) \equiv \rho(z, t) - \rho_o(z, t)$  is the atmospheric density perturbation,  $z$  is the altitude and  $t$  represents time.  $\rho(z_R, t)$  is the perturbed atmospheric density at a normalization altitude  $z_R = 40$  km, thus  $\rho(z, t)/\rho(z_R, t)$  is the perturbed relative density (relative to the atmospheric density at normalization altitude  $z_R$ ). The raw data resolutions are 48 m and 2.5 min. To improve the signal-to-noise ratio (SNR) in the GW analysis, the vertical resolution  $\Delta z$  is reduced to 192 m and the temporal resolution  $\Delta t$  is set to 5 min.

The background relative density  $\rho_o(z, t)/\rho(z_R, t)$  is estimated from a 3-h data window using the approach outlined in a companion paper (Yamashita et al., 2008) and similar to Hostetler and Gardner (1990). The obtained  $\rho_o(z, t)/\rho(z_R, t)$  is the sum of the unperturbed background density and perturbations induced by long-period waves (Yamashita et al., 2008). The relative density perturbation  $\rho'(z, t)/\rho(z_R, t)$  is then obtained by subtracting the estimated background  $\rho_o(z, t)/\rho(z_R, t)$  from each measured density profile  $\rho(z, t)/\rho(z_R, t)$  of 5-min integration. This background subtraction removes both the unperturbed background

and long-period waves (such as tides and stationary waves), leaving short-period waves (periods less than 6h—double the window length) in  $\rho'(z, t)/\rho(z_R, t)$ . To reduce the noise level (mainly with very short periods), the obtained relative density perturbation  $r(z, t)$  is low-pass filtered with a vertical cutoff wavelength  $\lambda_c$  of 2 km and a temporal cutoff period  $T_c$  of 60 min. Such filter and background windows allow us to calculate GWs with vertical wavelengths of 2–30 km and periods of 60–360 min. The resulted two-dimensional (2-D) relative density perturbations are for every 5 min through the entire dataset. Two examples of sequence plots are shown in Fig. 1 for the South Pole and Rothera, respectively.

The GW strength is then characterized by the root-mean-square (RMS) relative density perturbation. To do so, the mean-square (MS) relative density perturbation is calculated:

$$\langle r^2 \rangle = \frac{1}{TL} \int_0^T \int_0^L r^2(z, t) dz dt - \left[ \frac{1}{TL} \int_0^T \int_0^L r(z, t) dz dt \right]^2 \quad (2)$$

where  $T$  and  $L$  are the 2-D window sizes ( $T = 3$  h and  $L = 15$  km). The positive bias introduced by photon noise in the MS relative density perturbation must be subtracted to obtain the pure MS perturbation, i.e., the non-biased GW strength. Senft and Gardner (1991) gave a bias estimation equation for nighttime observations where the background noise can be neglected. We further develop the equation to account for the noise caused by the daytime solar background:

$$\begin{aligned} [\Delta r]_{\text{LPF}}^2 = & \frac{4\Delta t \Delta z}{T_c \lambda_c} \frac{1}{TL} \int_0^T \int_0^L \left\{ \frac{[\Delta N_T(z, t)]^2}{[N_T(z, t) - \hat{N}_B(t)]^2} \right. \\ & \left. + \frac{[\Delta N_T(z_R, t)]^2}{[N_T(z_R, t) - \hat{N}_B(t)]^2} \right\} dz dt \quad (3) \end{aligned}$$

where  $N_T(z, t)$  is the total photon count for each bin,  $\hat{N}_B(t)$  is the estimated background photon count, and  $[\Delta N_T(z, t)]_{\text{rms}} = \sqrt{N_T(z, t)}$  is the photon noise associated with  $N_T(z, t)$ . The RMS relative density perturbation, i.e., the GW strength, is computed as

$$(r)_{\text{rms}} = \sqrt{\langle r^2 \rangle_{\text{Pure}}} = \sqrt{\langle r^2 \rangle - [\Delta r]_{\text{LPF}}^2}. \quad (4)$$

GW spectrum analysis is performed on the 2-D relative density perturbations. A 2-D FFT is applied to derive the 2-D power spectral density (PSD). The vertical wavelength  $\lambda_z$  and corresponding period  $T$  of the dominant wave with the highest PSD are estimated from the PSD profile. The GW vertical phase speed  $c_z$  is then calculated as  $c_z = \lambda_z/T$ .

### 2.3. Criteria for GW data analysis

Four criteria are used for data quality control and GW identification. First, by checking the Rayleigh and background levels, any profiles taken under lidar beam alignment and cloudy conditions are removed. Second, due to the use of a 3-h window for background estimate, any data sets with a period less than 3 h are excluded from the GW data analysis. Third, the RMS uncertainty of  $\langle r^2 \rangle_{\text{Pure}}$  in the 3-h window must be smaller than 50% of  $\langle r^2 \rangle_{\text{Pure}}$ . This RMS uncertainty  $\phi$  is adapted from Senft and Gardner (1991):

$$\phi = \left[ \lambda_c T_c \overline{[\Delta r]_{\text{LPF}}^2} / TL \langle r^2 \rangle_{\text{Pure}} \right]^{1/2}. \quad (5)$$

Fourth, hourly data must show GW downward phase progression in order to be qualified in the GW database. Only data that pass all four criteria are used for this study.

## 3. Observations

Amundsen–Scott South Pole Station (90°S) is located at the Antarctic plateau. The lidar observations at the South Pole were made by the University of Illinois under the support of the National Science Foundation from December 1999 to October 2001. Rothera (67.5°S, 68.0°W) is located on Adelaide Island near the Antarctic Peninsula. The lidar observations at Rothera were a collaborative effort between the British Antarctic Survey and the University of Illinois from December 2002 to March 2005. PMCs were observed by the lidar from November to February during two austral summers (1999–2000 and 2000–2001) at the South Pole (Chu et al., 2003) and during three austral summers at Rothera (2002–2003, 2003–2004, and 2004–2005) (Chu et al.,

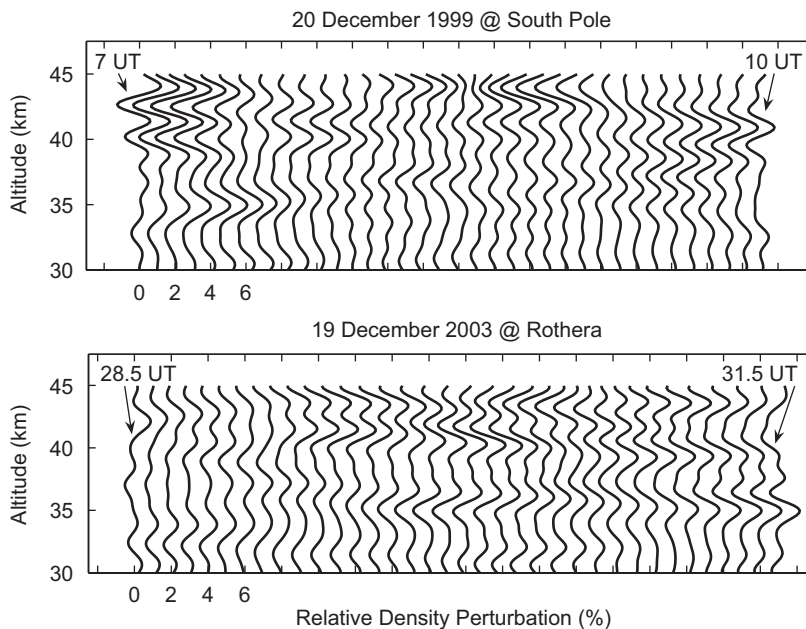


Fig. 1. Sequence plots of the 2-D filtered relative density perturbations obtained for 20 December 1999 at the South Pole and 19 December 2003 at Rothera. Each relative density profile represents an integration of 5-min data and is shifted by 1% to the right progressively.

2006). In order to study the GW–PMC correlation we analyze the lidar density data in the PMC season from November to February to derive stratospheric GW strength and spectrum in the altitude range of 30–45 km. This range is chosen for comparison with earlier studies by Gerrard et al. (1998, 2004a, b) at Sondrestrom, Greenland (67.0°N, 50.9°W). It is also in consideration of the SNR thus the reliability of the lidar data.

Statistics of examination and occurrence hours (and datasets) for PMC and GW are summarized in Table 1. The total hours of data that passed the first two criteria and used for examining GWs are ~399 h at the South Pole and ~354 h at Rothera. The large difference between the PMC and GW examination hours is partially due to the fact that many datasets shorter than 3 h are excluded from GW examination. Furthermore, many hours of data with relatively low Rayleigh signals or questionable overlapping between the lidar beam and the receiver field of view are also excluded from the GW analysis to ensure the data quality. GWs are observed in ~306 h at the South Pole and ~318 h at Rothera, i.e., these data pass the last two criteria and show clear GW signatures. About 93 and 36 h of data are disqualified at the South Pole and Rothera by the third criterion because the MS perturbations in these hours are not significantly larger than the uncertainty caused by photon noise. Histograms of the distribution of GW examination and occurrence hours versus UT are plotted in Fig. 2. Lidar observations cover the full diurnal cycle with relatively homogeneous distribution at the South Pole but inhomogeneous distribution at Rothera. Due to the high solar

background around noon hours at Rothera, the GW occurrence hours are biased towards local midnight (4.5 UT). There are 37 and 23 datasets with both PMC and GW occurrence at the South Pole and Rothera, respectively. Only these simultaneous datasets are used in the following derivation of correlation coefficients between GW strength and PMC brightness.

3.1. Correlations between GW strength and PMC brightness at different latitudes

Similar to the approach taken by Gerrard et al. (1998, 2004a), the correlation between GW strength and PMC brightness is characterized by a linear correlation coefficient (LCC) between the TBC of PMCs and the RMS relative density perturbation (RMS perturbation for short) of GWs. The LCC is defined as (Press et al., 1986):

$$LCC = \frac{\sum_i (r_i - \bar{r})(\beta_i - \bar{\beta})}{\sqrt{\sum_i (r_i - \bar{r})^2} \sqrt{\sum_i (\beta_i - \bar{\beta})^2}} \quad (6)$$

where  $r_i$  and  $\beta_i$  are the mean GW RMS perturbation and mean PMC TBC for each dataset  $i$ , and  $\bar{r}$  and  $\bar{\beta}$  are the means of  $r_i$  and  $\beta_i$  used in the LCC calculation, respectively. Dataset-mean values of TBC  $\beta_i$  and RMS perturbation  $r_i$  are used, instead of hourly or 3-h mean values. This is because the stratospheric GWs in the range of 30–45 km take about 10–20 h to propagate to the PMC region for vertical group velocity ~2–3 km/h. The hourly PMCs may not have a one-to-one correlation with hourly stratospheric waves but the overall dataset means could provide a clue whether these two are correlated (Gerrard et al., 1998). To take the dataset means, the TBC for the hours with waves but without clouds are set to zero.

Plotted in Figs. 3(a) and (b) are the PMC brightness versus GW strength for the South Pole and Rothera, respectively. Each data point in the figures represents a dataset-mean PMC TBC and GW RMS perturbation. The error bars on each point are the standard deviations of PMC TBC and the uncertainty of GW RMS perturbation within each dataset. The cutoff period and wavelength of the low-pass filters used for these figures are 60 min and 2 km. Without considering the standard deviations, the LCC derived

**Table 1**  
Summary of lidar observations of PMC and stratospheric GW at the South Pole and Rothera, Antarctica

	South Pole	Rothera
PMC examination hours/datasets	650 h/78 sets	459 h/46 sets
PMC occurrence hours/datasets	437 h/67 sets	128 h/32 sets
GW examination hours/datasets	399 h/54 sets	354 h/47 sets
GW occurrence hours/datasets	306 h/51 sets	318 h/47 sets
Simultaneous GW and PMC observation hours/datasets	222 h/37 sets	210 h/23 sets

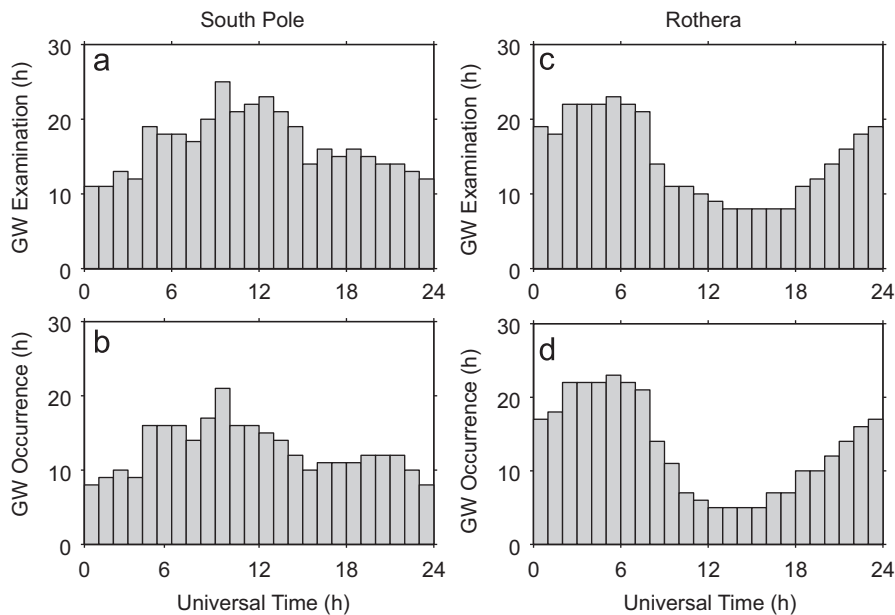


**Fig. 2.** Histograms of gravity wave examination and occurrence hours in the summer from November to February at the South Pole and Rothera, Antarctica.

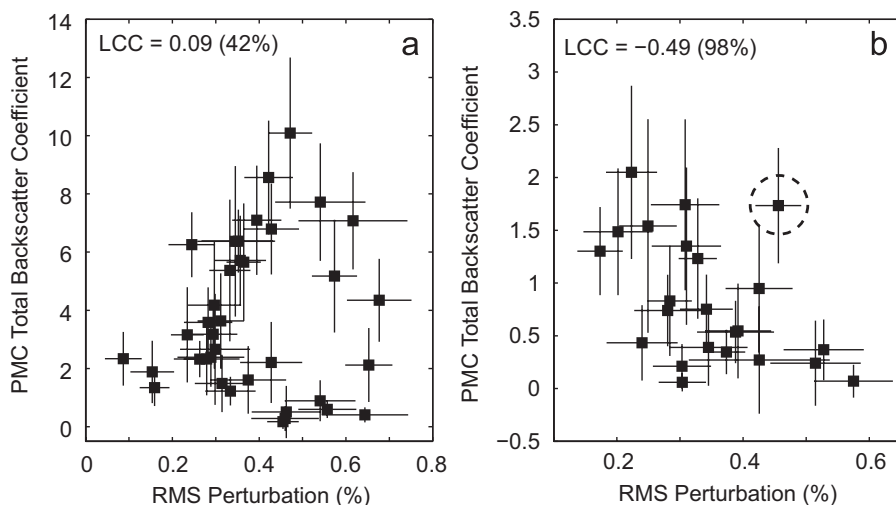


**Fig. 3.** PMC brightness (total backscatter coefficient) versus GW strength (RMS relative density perturbations in the 30–45 km range) at the South Pole (a) and Rothera (b). The gravity wave data were processed using a low-pass filter with a 60-min cutoff period. Each data point represents a dataset-mean PMC TBC and GW RMS perturbation. Error bars represent the uncertainty of GW RMS perturbation and standard deviation of PMC TBC. Circled data point represents 25 January 2003.

directly from the 37 and 23 data points in Figs. 3(a) and (b) are 0.09 with a 42% confidence level for the South Pole and  $-0.49$  with a 98% confidence level for Rothera. Using a Monte Carlo method similar to Gerrard et al. (2004a) to run the computation of LCC within the half standard deviation of each point for 100,000 times, the obtained mean LCC in the Monte Carlo method is  $0.09 \pm 0.05$  with a confidence level of 39% for the South Pole and  $-0.43 \pm 0.07$  with a confidence level of 95% for Rothera. Our results show that the PMC brightness and GW strength are uncorrelated at the South Pole, which can be seen from two aspects. First, the LCC is very close to zero, indicating no significant correlation. Second, a confidence level of 42% or 39% means that the probability of using two random data sets to obtain the same LCC is 58% or 61%, so the two datasets  $\{r_i\}$  and  $\{\beta_i\}$  are unlikely to be correlated. The negative correlation at Rothera given by the LCC is statistically significant as the confidence level is above 95%, i.e., the probability of getting a correlation as large as the observed value by random chance is less than 5%. Therefore, our lidar observations show that the stratospheric GW strength is negatively correlated with the PMC brightness at Rothera but no significant correlation exists at the South Pole.

The dataset-mean GW RMS perturbations in Fig. 3(b) for Rothera distribute from 0.1% to 0.6% with most of the data points below 0.4%. The points with lower PMC brightness tend to be at larger GW RMS perturbation and the points with higher PMC brightness tend to distribute at smaller GW RMS perturbation, except one point whose TBC is high around  $1.7 \times 10^{-6} \text{ sr}^{-1}$  but its corresponding RMS perturbation is also quite high around 0.45%. This exceptional point is 25 January 2003 when the Columbia shuttle exhaust reached Rothera station, potentially enhancing the PMC occurrence and brightness as discovered by Stevens et al. (2005). Excluding this point from the LCC calculation, we obtain a Rothera LCC of  $-0.61$  with a confidence level of 99%. Thus, the negative correlation becomes even stronger at Rothera. The distribution of the dataset-mean GW RMS perturbations in Fig. 3(a) for the South Pole is from 0.05% to 0.70%, slightly larger than the Rothera distribution range. The dataset-mean PMC TBC at the South Pole is 4–5 times brighter than that at Rothera. There is no clear trend in the entire distribution for the South Pole. While the right side points show random distribution, a positive correlation is apparent among the left-side data points in Fig. 3(a).

If the correlation is derived using only the data on the left side, the LCC goes to  $+0.74$  with a confidence level of 99.98%. This subset data cover both seasons (1999–2000 and 2000–2001) and distribute in all 3 months (December, January, and February). No specific year or month or time of day dominates this positive correlation. For the rest of the data on the right side that form a near-circle shape, they are also from different seasons and months. The overall effect of all data points shows no significant correlation but this subset exercise indicates a possibility of different populations of ice particles having different responses to GW perturbations at the South Pole.

### 3.2. Correlations for different GW spectra

The results in Section 3.1 are obtained with a low-pass filter cutoff period of 60 min and a background window of 3-h. Thus, the periods of the GWs detected in the 30–45 km range from 60 to 360 min. Decreasing the low-pass filter cutoff period to 30 min will allow more waves with shorter periods to be included in the RMS perturbation. The shorter-period waves have larger vertical phase speed if similar vertical wavelength can be assumed for different wave spectra. If one further assumes that the vertical group velocity is equal to the observed vertical phase speed but is of the opposite direction, the shorter-period waves will be less likely to encounter critical levels than the longer-period waves. Thus shorter-period waves have a greater chance of reaching the PMC region, and if the Rothera negative correlation is true, we expect a stronger negative correlation when shorter-period waves are included. As for the South Pole, we expect no significant changes in the correlation when the cutoff period is varied.

We perform the GW spectrum tests in the 30–45 km as follows. The temporal low-pass filter cutoff period is varied from 60-min to 30- and 90-min, respectively while the spatial low-pass filter cutoff wavelength (2 km) is kept the same as before. The rest of the steps are the same as in the case of 60-min cutoff. In all cases we allow the third criterion to remove data points whose uncertainty is larger than 50% of the RMS perturbation itself. This criterion is applied because both waves and noise can change with the cutoff period. In fact, the mean signal-to-noise ratio decreases in the 30-min cutoff case when compared to the 60-min case. Fortunately, Eq. (3) correctly estimates the bias caused by

the solar background so the RMS relative density perturbations derived from Eq. (4) for the 30-min cutoff case are still reliable enough for the correlation study. The obtained LCCs for 30-, 60-, and 90-min cutoff are summarized in Tables 2 and 3 for the South Pole and Rothera, along with the corresponding confidence levels. For Rothera, the LCCs derived from the 23 data points without considering the standard deviations are  $-0.54$ ,  $-0.49$ , and  $-0.46$  with confidence levels of 99%, 98%, and 97% for the three cases with cutoff periods of 30-, 60-, and 90-min, respectively. Running Monte Carlo tests within half of the standard deviations for 100,000 times, the obtained mean LCCs are  $-0.49 \pm 0.07$ ,  $-0.43 \pm 0.07$ , and  $-0.40 \pm 0.09$  with 97%, 95%, and 92% confidence levels for 30-, 60-, and 90-min cases. Thus, our tests indicate that the negative correlation increases with a shorter cutoff period. Fig. 4 shows the PMC brightness versus GW strength for the cases of 30- and 90-min cutoff periods. Comparing Fig. 4 with Fig. 3, it is clear that the average RMS relative density perturbation in the shorter-period cutoff case is larger than the longer-period case because more GWs are included in the shorter-period case. The increase trends of both the correlation and the GW RMS perturbation are consistent with our expectation, implying the true negative correlation between GW strength and PMC brightness at Rothera. For the South Pole, some data points are removed by the third criterion for the 90-min cutoff period case. This may be understood as while the larger window reduces noise, shorter-period waves are removed more, leading to insignificant RMS perturbation. Fig. 4 shows that the average RMS perturbation

increases with the shorter cutoff period while the LCCs remain at near-zero values in all three cases. This is consistent with our expectation, indicating no significant correlation at the South Pole.

#### 4. Discussion

Comparing our results with previous studies by Gerrard et al. (2004a) at Sondrestrom in the northern hemisphere, the Rothera correlation coefficients are very similar to or slightly larger than those at Sondrestrom. Gerrard et al. (2004a) used the peak VBC to represent the PMC brightness and found the LCC between PMC peak VBC and GW RMS relative density perturbation to be  $-0.44$  with a confidence level of 95% from the data points and  $-0.35$  with a confidence level of 95% from the Monte Carlo method. Why does the negative correlation exist at Rothera and Sondrestrom but no significant correlation exists at the South Pole? In the following we investigate the problem from three aspects: (1) the stratospheric GW strength and spectrum in 30–45 km (wave source for PMC region), (2) whether these waves can reach the PMC region (wave propagation and breaking), and (3) how GWs reaching the PMC region affect PMC brightness under different background conditions (PMC microphysics).

##### 4.1. Stratospheric GW strength and spectrum in the 30–45 km altitude range

The first question to ask is whether the stratospheric GWs in the 30–45 km are much weaker at the South Pole than at the two other locations. Weaker waves in 30–45 km could lead to weaker waves at PMC region, resulting in no significant influence on PMCs. The means and standard deviations of the dataset-mean RMS perturbation in Figs. 3(a) and (b) are  $0.39 \pm 0.14\%$  and  $0.35 \pm 0.11\%$  for the South Pole and Rothera, respectively. This indicates that the GW strengths on PMC days are comparable in the 30–45 km range at these two locations. To further examine the GW strength we plot in Fig. 5 the histograms of GW RMS relative density perturbation for Rothera and the South Pole: the total data in summer from November to February on the left column; the values on the days with PMC occurrence (middle column); and the days without PMC occurrence (right column). Each count in Fig. 5 represents the RMS perturbation in a 3-h window. On PMC days Rothera exhibits a preference of small RMS perturbations while the South Pole has a relatively homogeneous distribution. For no PMC days the RMS perturbations are spread out at the South Pole from 0.1% to 0.9% while more tightly clustered at Rothera. As summarized in Table 4, the mean GW strengths are comparable within the standard deviations between Rothera and the South Pole. The observed GW strength and its distributions at Rothera are very similar to the results at Sondrestrom (Gerrard et al., 2004a). Thus, the GW strengths in 30–45 km are comparable among all three locations during the summer. This result is quite surprising at first, as Rothera should have much stronger orography GW sources than the South Pole. As analyzed in a companion paper (Yamashita et al., 2008), the similar strength in the stratosphere between Rothera and the South Pole occurs only in summer. During winter months, the Rothera GW potential energy densities are  $\sim 4$  times larger than those at the South Pole. The disparity between seasons is most likely due to different critical level filtering effects at the two locations between seasons. Yamashita et al. (2008) suggest that in summer the critical levels between the troposphere and the stratosphere filter out most orography-generated GWs, resulting in similar GW strengths between the two sites. The critical level filtering at Rothera is minimum in winter, allowing most orography GWs to reach the

**Table 2**  
South Pole linear correlation coefficients between PMC brightness and GW strength in the 30–45 km

South Pole (30–45 km)			
GW period (min)	30 <sup>a</sup> –360	60–360	90–360
GW wavelength (km)	2–30	2–30	2–30
Number of data points	39	37	35
Direct data-point method			
LCC	0.09	0.09	0.11
Confidence level (%)	40	42	49
Monte Carlo method (100,000 times run)			
LCC $\pm$ std.	$0.08 \pm 0.05$	$0.09 \pm 0.05$	$0.11 \pm 0.05$
Confidence level (%)	38	39	45

<sup>a</sup> 30, 60, and 90 min are the different cutoff periods of the low-pass filters used in GW data analysis.

**Table 3**  
Rothera linear correlation coefficients between PMC brightness and GW strength in the 30–45 km

Rothera (30–45 km)			
GW period (min)	30 <sup>a</sup> –360	60–360	90–360
GW wavelength (km)	2–30	2–30	2–30
Number of data points	23	23	23
Direct data-point method			
LCC	$-0.54$	$-0.49$	$-0.46$
Confidence level (%)	99	98	97
Monte Carlo method (100,000 times run)			
LCC $\pm$ std.	$-0.49 \pm 0.07$	$-0.43 \pm 0.07$	$-0.40 \pm 0.09$
Confidence level(%)	97	95	92

<sup>a</sup> 30, 60, and 90 min are the different cutoff periods of the low-pass filters used in GW data analysis.

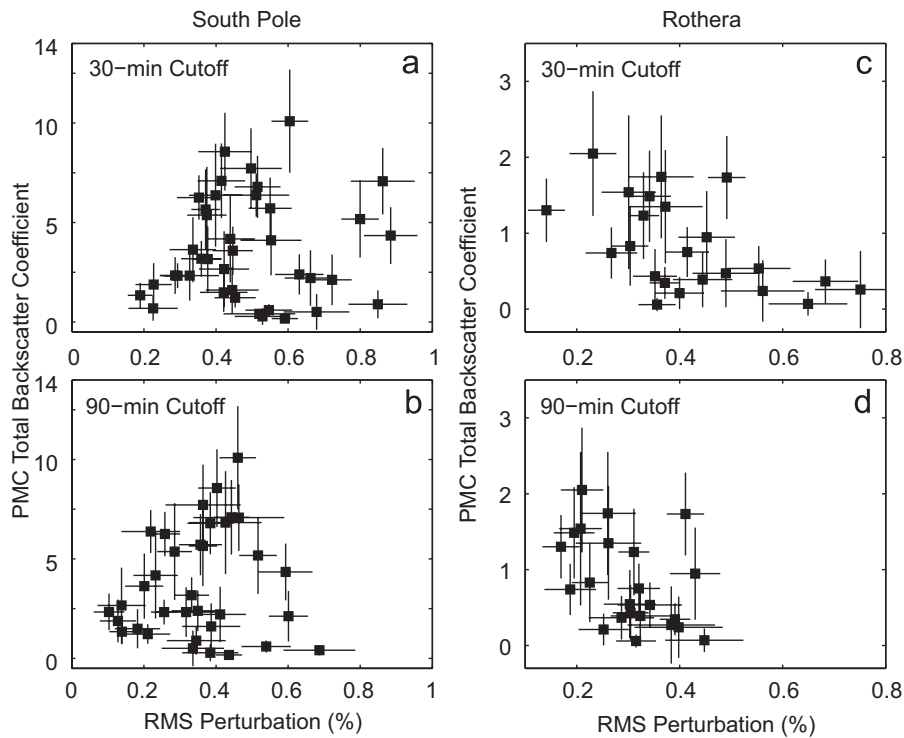


**Fig. 4.** PMC total backscatter coefficient versus GW RMS relative density perturbations in the 30–45 km range at the South Pole (a, b) and Rothera (c, d) for 30-min cutoff period (a, c) and for 90-min cutoff period (b, d). Each data point represents a dataset-mean PMC TBC and GW RMS perturbation. Error bars represent the uncertainty of GW RMS perturbation and standard deviation of PMC TBC.

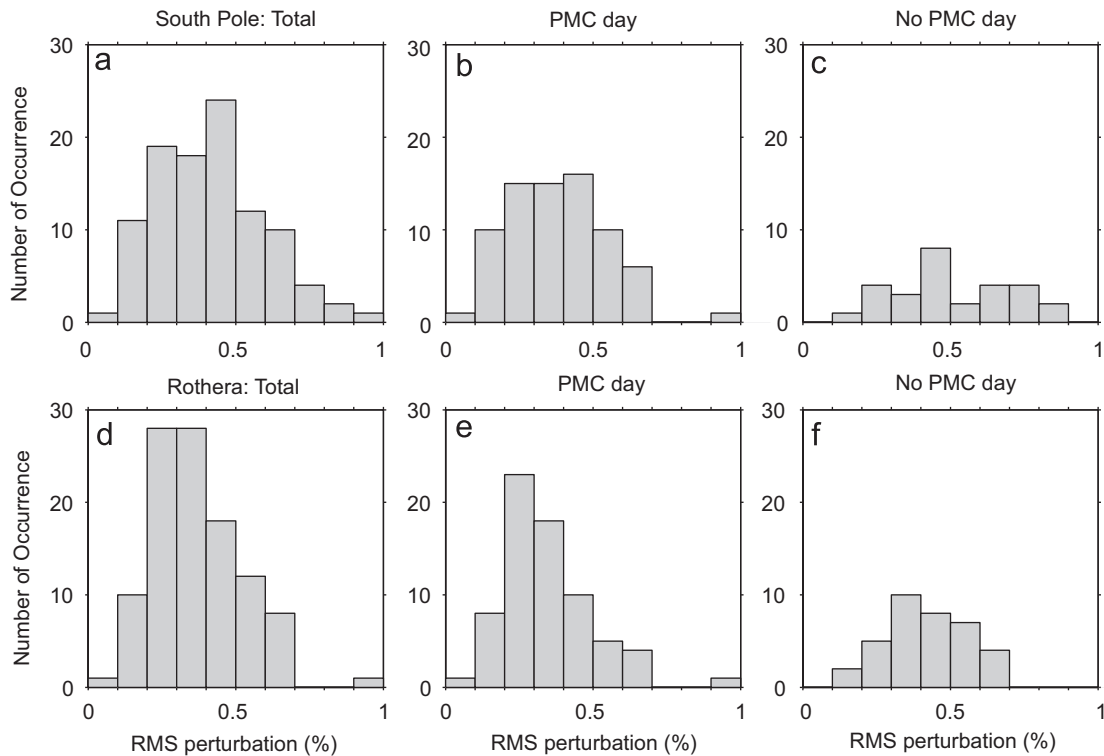


**Fig. 5.** Comparison of summer gravity wave strengths at the South Pole (upper panels) and Rothera (lower panels): total summer data (a, d), on days with PMC occurrence (b, e), and on days without PMC (c, f). Data were analyzed using a low-pass filter with a 60-min cutoff period and a 2-km cutoff wavelength. Each data point represents a 3-h data.

30–45 km range. Polar vortex and stratospheric jet streams may also contribute to the winter enhancement of GW strength at Rothera (Yamashita et al., 2008).

The next question to ask is whether the South Pole has different GW spectra than Rothera. GWs with different spectra may have different chances to approach the critical levels in

**Table 4**  
Statistics of stratospheric GW strength in summer at the South Pole and Rothera

	South Pole			Rothera		
	Total	PMC day	No PMC day	Total	PMC day	No PMC day
Observation (h)	306	222	84	318	210	108
Observation (dataset)	51	37	14	47	23	24
RMS <sup>a</sup> (%) (mean±std) <sup>b</sup>	0.42±0.18	0.38±0.17	0.51±0.19	0.37±0.15	0.34±0.15	0.41±0.15

<sup>a</sup> RMS means the RMS relative density perturbation in the 30–45 km.

<sup>b</sup> The mean and std are the mean and standard deviation of 3-h data points.

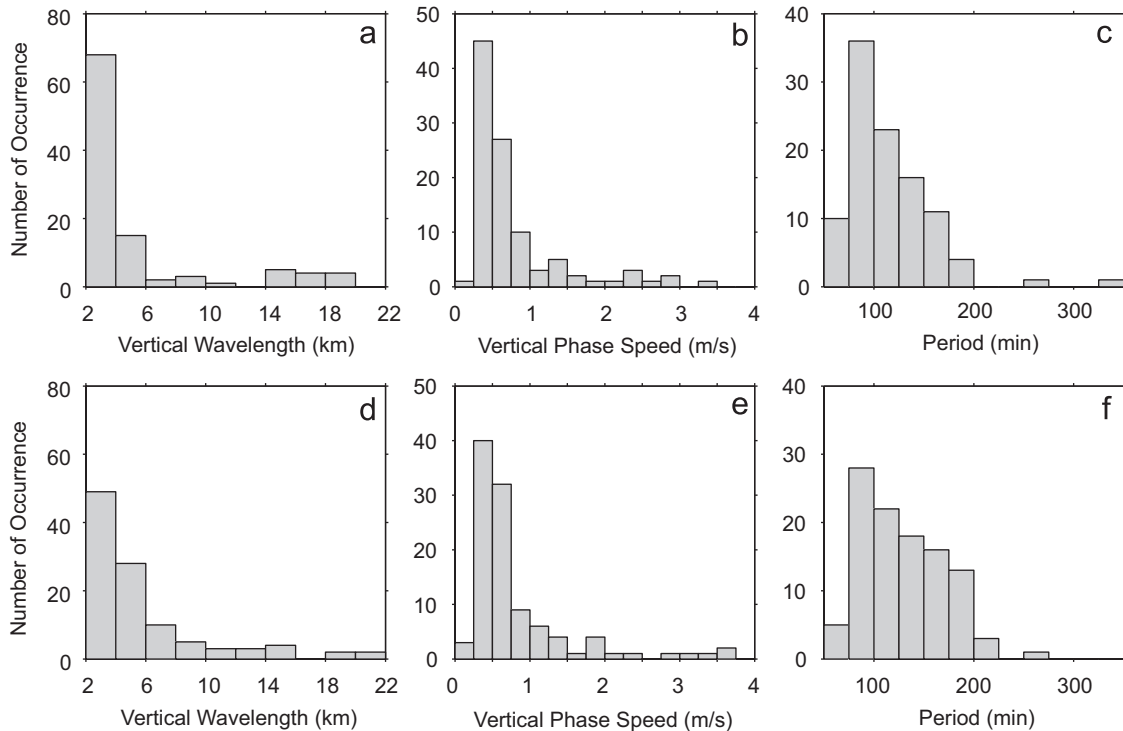


**Fig. 6.** Comparison of stratospheric gravity wave spectra in the 30–45 km altitude region between the South Pole (top) and Rothera (bottom): vertical wavelength (a, d), vertical phase speed (b, e), and period (c, f). Data were analyzed using a low-pass filter with a 60-min cutoff period and a 2-km cutoff wavelength. Each data point represents a 3-h data.

between the stratosphere and the mesosphere. Different spectra of GWs may also have different effects on PMC microphysics. Illustrated in Fig. 6 are the histograms of summer GW vertical wavelengths, vertical phase speeds, and periods obtained for Rothera and the South Pole in the 30–45 km. Each count represents a 3-h value. The distributions of vertical wavelengths and periods at Rothera are similar to those at the South Pole but slightly biased to longer wavelengths and periods. Both locations have similar distributions of vertical phase speeds. Summarized in Table 5 are the mean characteristics of summer GWs in the 30–45 km at the South Pole and Rothera. Within standard deviations the South Pole and Rothera have comparable GW spectra. The mean vertical phase speeds of  $0.77 \pm 0.65$  and  $0.80 \pm 0.72$  m/s for the South Pole and Rothera are also similar to Sondrestrom results of 0.56–0.83 m/s (2–3 km/h). By definition the vertical group velocity of GWs is equal to the intrinsic vertical phase speed but with an opposite sign. The ground-based lidars observe the ground-relative phase speed, not the intrinsic phase speed. When assuming the observed and intrinsic frequencies are similar, the observed vertical phase speed can be regarded as the vertical group velocity of the waves. Such assumption is reason-

able if the background wind is smaller than the wave horizontal phase speed. Due to the lack of background wind and horizontal wavenumber information, our results stated above are under such assumption. The similar GW strength and spectrum in the 30–45 km cannot account for the different correlations at Rothera and the South Pole.

#### 4.2. Wave propagation from the stratosphere to the mesopause region

The third question to ask is whether the stratospheric waves can reach the PMC regions. This question involves two issues—whether the waves are filtered out during propagation by the critical levels between the stratosphere and the PMC region and whether the waves break before reaching PMC altitudes. Our lidar data cannot provide information on either of these issues. NASA/UARS Reference Atmosphere Project provides a baseline standard zonal wind model (Swinbank and Ortland, 2003). It shows the mesospheric jet offset from the South Pole in summer with considerably stronger zonal wind at the latitude of Rothera

**Table 5**  
Statistics of stratospheric GW spectrum in summer at the South Pole and Rothera

	South Pole			Rothera		
	Vertical wavelength (km)	Period (min)	Vertical phase speed (m/s)	Vertical wavelength (km)	Period (min)	Vertical phase speed (m/s)
Mean $\pm$ std <sup>a</sup>	5.2 $\pm$ 4.8	115 $\pm$ 42	0.77 $\pm$ 0.65	5.7 $\pm$ 4.4	128 $\pm$ 40	0.80 $\pm$ 0.72
Range—min—max	2.0–19.7	67–341	0.17–3.37	2.0–21.8	67–269	0.19–3.58

<sup>a</sup> The mean and std are the mean and standard deviation of 3-h data points.

than at the South Pole. As a result, vertically propagating GWs over Rothera would encounter a wide range of wind velocities compared with the weak stratospheric and mesospheric winds over the pole. Sondrestrom in the northern hemisphere has similar westward wind patterns as Rothera in summer. Therefore, the South Pole is unlikely to have stronger critical level filtering effects from the stratosphere to the mesopause than Rothera and Sondrestrom if we assume the wave propagation directionality relative to background wind being similar among three stations.

The wave directional information is very important in determining whether the stratospheric waves can affect overlying PMCs (Gerrard et al., 2004b). The critical level is reached only when the wave vector is the same as the background wind. If GWs at the South Pole were filtered out before reaching the PMC region, there would be no correlation between PMCs and GWs. Although possible, it is unlikely the case from a statistical point of view. If waves propagate horizontally away from the observation site, they may not affect overlying PMCs. With a ray tracing model Gerrard et al. (2004b) showed that the waves observed at  $\sim 40$  km were part of the same wave field affecting PMCs  $\sim 80$  km at Sondrestrom. They also showed that the wave breaking effect on PMCs discussed by Fritts et al. (1993) and Gerrard et al. (2004a) was largely absent for many waves simulated in their model. Lack of horizontal wave propagation information for the South Pole and Rothera prevents us from drawing any conclusions on the wave propagation issue. We do not know whether Rothera and the South Pole have the same amplitudes of GWs at the mesopause altitudes. We would like to measure and better model them in future studies.

#### 4.3. GW influences on PMC microphysics

We now turn our attention to the issue of how the GWs that reach the PMC region influence PMC under different background conditions. Jensen and Thomas (1994) pointed out that the GW effects on PMCs are twofold: the dynamical effects due to wave-induced wind perturbations, and the microphysical effects due to wave-induced temperature perturbations. The wave-induced wind perturbations can cause the undulation of PMC layers and cause the convergence and divergence of the number density of PMC particles. These mechanisms could be responsible for the wave structures in NLC observed from the ground with very low elevation angles (see Figs. 1 and 2 of Jensen and Thomas, 1994). However, excluding changes in cloud microphysical properties caused by wave dynamics, the dynamical effects should not alter the lidar-measured PMC TBC for two reasons. First, the lidar beam was pointed vertically and TBC is the integration of the entire PMC layers. Thus, the altitude shift of PMC layers will not affect the obtained TBC. Second, our statistical study takes the dataset-mean TBC so the periodic convergence and divergence effects of particle number density will be averaged out. Therefore, if the lidar observes any correlation between PMC and GW, it has to come from the microphysical effects driven by the wave-induced

temperature perturbations. Rapp et al. (2002) included GWs in 2-D simulations of PMC formation using wave parameters determined from lidar measurements. They showed that the wave-driven wind and temperature perturbations could modulate ice crystal sizes and PMC optical properties. They concluded that GWs with periods longer than 6.5 h tend to amplify PMC brightness, whereas shorter waves tend to destroy the clouds. Thayer et al. (2003) concluded based on observations that GWs with periods of 2–3 h reduce PMC brightness.

Before analyzing how GWs influence PMC microphysics, we want to point out the obvious differences among the three sites—PMCs at the South Pole are much brighter and more frequent than the clouds at Rothera and Sondrestrom. Chu et al. (2003, 2006) reported the means of hourly PMC TBC being  $5.43 \times 10^{-6} \text{sr}^{-1}$  for the South Pole and  $2.34 \times 10^{-6} \text{sr}^{-1}$  for Rothera. The mean of hourly PMC TBC at Sondrestrom, after converted to 374 nm as used by the Fe Boltzmann lidar, is  $2.46 \pm 2.30 \times 10^{-6} \text{sr}^{-1}$ , comparable to the PMC brightness at Rothera (Chu et al., 2006). Chu et al. (2003) reported an occurrence frequency of 67.4% over the entire PMC season, and PMCs occur nearly 100% of the time in the middle of the season at the South Pole. Rothera and Sondrestrom only have around 20% occurrence frequency (Chu et al., 2006; Thayer and Pan, 2006). The differences in PMC brightness and occurrence frequency are a reflection of the differences in the background atmospheric conditions. Temperature and water vapor are the two key factors in determining the formation, development, and sublimation of PMC ice particles. TIME-GCM simulation shows that the South Pole summer temperatures at mesopause altitude ( $\sim 87$  km) are about 10–15 K colder than those at Rothera latitude (Xu et al., 2007) while SABER measurements (version 1.06) show that the December mesopause at  $67.5^\circ\text{S}$  is about 5 K warmer than the mesopause at  $85^\circ\text{S}$  (Xu et al., 2007). The version 1.07 of SABER data exhibits that the mesopause temperature difference between  $80^\circ\text{S}$  and  $67.5^\circ\text{S}$  is increased to 12–15 K, very similar to the TIME-GCM simulations, although there are discrepancies in the absolute temperatures between SABER and TIME-GCM (Jiyao Xu, State Key Laboratory of Space Weather, Chinese Academy of Sciences, private communication, 2008). Thus, it is clear that the South Pole summer mesopause region is much colder than that of Rothera and Sondrestrom. Assuming the same water vapor mixing ratio (reliable measurements of the global distribution of water vapor mixing ratio in MLT region are not available), the South Pole has much larger supersaturations with respect to ice than Rothera and Sondrestrom. Thus, more and/or larger ice particles can form at the South Pole, leading to brighter clouds.

As an air parcel rises and falls under the influence of a GW, the corresponding expansion and compression will induce adiabatic cooling and warming, leading to an oscillation of the air parcel temperature. In the typical summertime conditions at PMC altitudes, water vapor saturation with respect to ice occurs around 150 K. If the parcel temperature oscillates around a mean slightly lower than 150 K, the PMC ice particles inside the air parcel will experience temperatures above 150 K (subsaturated air) for part of

the oscillation period and below 150 K (supersaturation) for the rest of the period. Due to the exponential dependence of the equilibrium water vapor pressure (i.e., the saturation vapor pressure) on temperature, the sublimation of the ice particles in the subsaturated period is much faster than the growth by water vapor deposition on the ice surfaces in the supersaturated period. Thus, the effect of the waves is to reduce particle size and decrease PMC brightness. This mechanism can explain the negative influences of short-period GWs on mature PMCs. Here the short period is relative to the PMC growth timescale: when the PMC growth timescale is much longer than the wave period, the growth in the cold phase of the wave is very minor compared to the sublimation in the warm phase. Besides destroying mature PMC ice particles, GWs can also prevent new PMC formation. Jensen and Thomas (1994) found from their model test that the mesopause region temperatures had to be 5 K colder for PMC to form when GWs present. However, regardless of shifts in the mesospheric temperature profile, maximum PMC brightness will occur at the height where the saturation ratio is unity and ice crystals reach their maximum size. Hence, the influence of GWs on mature PMCs will likely be similar at Rothera and the South Pole.

The negative GW–PMC correlations observed at Rothera and Sondrestrom may be a result of relatively warm temperatures (and correspondingly low supersaturations) in the altitude region between the PMC altitude and the mesopause where ice crystals grow and sediment. If the supersaturations are small, then GW temperature perturbations can drive subsaturation in the warm phase of the wave, which could either reduce the size of ice crystals present or completely sublimate them. Ultimately, the PMC resulting from the sedimenting ice crystals will have diminished brightness even if the ice crystals survive to make a cloud. In contrast, at the South Pole where it is much colder in the region between the PMCs and the mesopause, supersaturations are generally large, ice crystals will continue growing even with GW temperature perturbations, and the impact of GW on PMC brightness will be relatively weaker than at Rothera. This hypothesis is consistent with the much higher PMC occurrence frequency at the South Pole than at Rothera. A schematic is shown in Fig. 7 to illustrate the above idea.

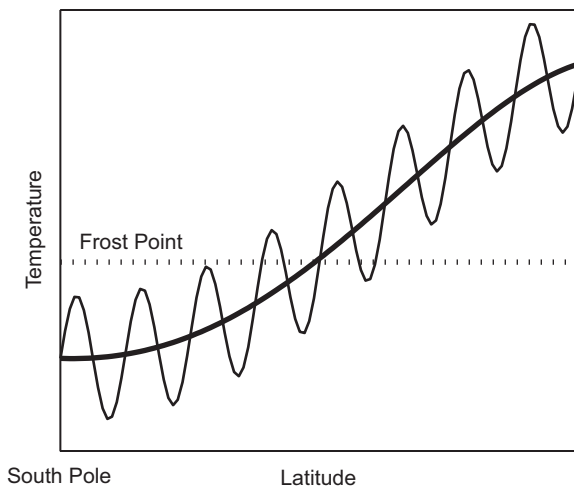


**Fig. 7.** A schematic to illustrate the idea of how the background temperatures in the ice crystal growth-sedimentation region between the PMC altitude and the mesopause influence PMC responses to gravity waves at different latitudes: A snapshot of the gravity wave perturbed temperatures versus latitudes. The thicker solid-line is the background temperature in this region, the periodic oscillation represents the GW-induced temperature perturbation, and the dotted line indicates the frost point temperature ( $\sim 150$  K) for typical summertime conditions in mesopause region.

It is also likely that gravity-wave-induced temperature perturbations will increase the number density of ice crystals nucleated in the mesopause region. Regardless of whether meteor smoke particles or proton-hydrate ions are the dominant ice nuclei, the number of ice crystals nucleated increases rapidly with decreasing temperature (Rapp and Thomas, 2006). Since wave-driven temperature perturbations decrease the minimum temperatures, they will cause sporadic nucleation of larger ice concentrations than would occur without the waves. However, the backscatter coefficient is proportional to the fifth or sixth power of radius. Thus, for a given ice mass in the clouds, increasing the number of ice crystals (and correspondingly decreasing their size) should decrease the cloud brightness. It should be noted here that we are examining the correlation between GW and PMC brightness directly overhead. Ice nucleation events and the resulting PMCs are often separated by large times and distances (Berger and von Zahn, 2007). Hence, even if GWs have a strong influence on ice nucleation processes, one might not expect to see a correlation in the zenith lidar data.

Even if the atmosphere is highly supersaturated over the South Pole such that GWs do not drive sublimation in the ice crystal growth-sedimentation altitude region, the wave-driven temperature perturbations will still modulate the ice crystal growth rates. Given the nonlinearity of the Clausius–Clapeyron vapor pressure temperature dependence, the temperature fluctuations will tend to decrease the mean particle size. However, the increased growth rates in the cold phase of the waves and decreased growth rates in the warm phase could also increase the width of the ice crystal size distribution. Given the extremely strong dependence of PMC brightness on particle size discussed above, it is possible that a wave-driven extension of the tail of the size distribution on the large end has a more important effect on mean PMC brightness than the decrease in mean particle size. Although this mechanism is purely speculative and microphysical modeling will be required to test the hypothesis, it might provide an explanation for the population of the data points at the South Pole suggesting a positive correlation between GW strength and PMC brightness.

## 5. Conclusions

Fe Boltzmann lidar data collected from the South Pole and Rothera ( $67.5^{\circ}\text{S}$ ), Antarctica are used to study the PMC brightness response to stratospheric GW perturbations in the 30–45 km. The PMC brightness is represented by the TBC of PMC layers and the GW strength is expressed through the RMS relative density perturbation in the 30–45 km range. A LCC is derived between the PMC TBC and the GW RMS perturbation to characterize the GW–PMC correlation. With the 60-min cutoff period and 2-km cutoff wavelength low-pass filter, a negative LCC of  $-0.49$  with a 98% confidence level is found between GW strength and the PMC brightness at Rothera, while the LCC at the South Pole is  $0.09$  with an 42% confidence level. The negative correlation coefficient at Rothera increases to  $-0.54$  (99%) with the 30-min cutoff period and decreases to  $-0.46$  (97%) with a 90-min cutoff. The South Pole correlation coefficient remains near zero through all cases. Therefore, the lidar observations show that the PMC brightness is negatively correlated with the stratospheric GW strength in the 30–45 km at Rothera while there is no significant correlation at the South Pole. The negative correlation at Rothera is statistically significant as the confidence level is above 95% and it is also similar to or slightly larger than the correlation observed at Sondrestrom ( $67.0^{\circ}\text{N}$ ), Greenland.

Our lidar observations show that GW strength and spectrum in the 30–45 km are comparable among the South Pole, Rothera, and

Sondrestrom in summer. For the GWs that reach the PMC region, the dynamical effects, i.e., the wave-induced wind perturbations, cannot alter the lidar-measured TBC (i.e., PMC brightness) so they are not responsible for the observed correlation. The lidar observed GW-PMC correlation is most likely a result of the microphysical effects driven by the wave-induced temperature perturbations. The different PMC brightness responses to GWs are likely caused by the different background temperatures in the ice crystal growth-sedimentation region between the PMC altitude (~84–85 km) and the mesopause (~88 km). As the Rothera temperatures in this region are typically not far below the frost point, the GW-induced temperature perturbations can drive subsaturation in the warm phase, destroying or limiting the growth of sedimenting ice crystals, and diminishing cloud brightness. This mechanism can explain the negative response at Rothera. However, the South Pole mesopause temperature is much colder and well below the frost point in the mesopause region. GW-perturbed temperatures may never be above the frost point. Thus, GWs may have a relatively weaker impact on PMC brightness at the South Pole than at Rothera. It is also possible that GWs are filtered out before reaching PMC region thus leading to no correlation between PMCs and GWs at the South Pole. Also, if waves propagate horizontally away from the observation site, they may not affect the overlying PMCs. Lack of background wind and wave propagation directional information prevents us from drawing any conclusions on the wave propagation issue. This should be addressed by future studies.

This study provides the first observational proof that PMC brightness responds to stratospheric GWs differently at different latitudes. This is very likely due to the latitudinal differences in background temperatures. At very high latitudes (~80°) when the mesopause temperature is far below the frost point, GWs may have very little influence on PMC brightness, similar to what we observed at the South Pole. Consequently, no GW signatures would be seen on PMC brightness. This may explain the phenomena observed by AIM/CIPS that wave signatures are not seen on PMC images at high latitudes but are very evident at NLC latitudes (Chandran et al., 2008). The proposed mechanisms above, including GW influence on ice particle nucleation, need to be verified through future modeling of gravity-wave effects on PMC. Furthermore, the different populations of ice particles at the South Pole indicated by the lidar observations await theoretical explanations and future modeling.

## Acknowledgements

We sincerely acknowledge David J. Maxfield, Jan C. Diettrich, and the staff of the British Antarctic Survey and the Rothera Research Station for their support through the entire campaign at Rothera. We also acknowledge two winter-over scientists, Ashraf El Dakrouri and John Bird, and the staff of Amundsen-Scott South Pole Station for their help and support in collecting data at the South Pole. We appreciate the valuable discussion with Gary E. Thomas and Hans G. Mayr. We sincerely acknowledge Jiyao Xu for providing us the temperature comparison results with SABER version 1.07 data. We are very grateful to Chester S. Gardner, George C. Papen, Robert Kerr and Robert Robinson for their inspiration and support. The Rothera lidar project was supported by the UK Natural Environmental Research Council and by the United States National Science Foundation (NSF) Grant ATM-0602334. X.C., C.Y., and W.H. were partially supported by NSF CAREER Grant ATM-0645584, NSF CEDAR Grant ATM-0632501, and NSF CRRL Grant ATM-0545353. C.Y. sincerely acknowledges the generous support of NCAR Newkirk Graduate Fellowship. H.L.L.'s effort is in part supported by the Office of Naval Research

(N00014-07-C0209). National Center for Atmospheric Research is sponsored by the National Science Foundation.

## References

- Berger, U., von Zahn, U., 2007. Three-dimensional modeling of the trajectories of visible noctilucent cloud particles: an indication of particle nucleation well below the mesopause. *Journal of Geophysical Research* 112, D16204.
- Chandran, A., Rusch, D.W., Palo, S.E., Thomas, G.E., Taylor, M.J., 2008. Gravity wave observations in the summertime polar mesosphere from the Cloud Imaging and Particle Size (CIPS) experiment on the AIM spacecraft. *Journal of Atmospheric and Solar-Terrestrial Physics*, this issue.
- Chanin, M.-L., Hauchecorne, A., 1981. Lidar observations of gravity and tidal waves in the stratosphere and mesosphere. *Journal of Geophysical Research* 86, 9715–9721.
- Chu, X., Gardner, C.S., Papen, G., 2001a. Lidar observations of polar mesospheric clouds at South Pole: seasonal variations. *Geophysical Research Letters* 28, 1203–1206.
- Chu, X., Gardner, C.S., Papen, G., 2001b. Lidar observations of polar mesospheric clouds at South Pole: diurnal variations. *Geophysical Research Letters* 28, 1937–1940.
- Chu, X., Pan, W., Papen, G., Gardner, C.S., Gelbwachs, J., 2002. Fe Boltzman temperature lidar: design, error analysis, and initial results at the North and South Pole. *Applied Optics* 41, 4400–4410.
- Chu, X., Gardner, C.S., Roble, R.G., 2003. Lidar studies of inter annual, seasonal and diurnal variations of polar mesospheric clouds at the South Pole. *Journal of Geophysical Research* 108 (D8), 8447.
- Chu, X., Nott, G.J., Espy, P.J., Gardner, C.S., Diettrich, J.C., Clilverd, M.A., Jarvis, M.J., 2004. Lidar observations of polar mesospheric clouds at Rothera, Antarctica (67.5°S, 68.0°W). *Geophysical Research Letters* 31, L02114.
- Chu, X., Espy, P.J., Nott, G.J., Diettrich, J.C., Gardner, C.S., 2006. Polar mesospheric clouds observed by an iron Boltzmann lidar at Rothera (67.5°S, 68.0°W), Antarctica from 2002–2005: properties and implications. *Journal of Geophysical Research* 111, D20213.
- DeLand, M.T., Shettle, E.P., Thomas, G.E., Olivero, J.J., 2003. Solar backscattered ultraviolet (SBUV) observations of polar mesospheric clouds (PMCs) over two solar cycles. *Journal of Geophysical Research* 108 (D8), 8445.
- DeLand, M.T., Shettle, E.P., Thomas, G.E., Olivero, J.J., 2007. Latitude-dependent long-term variations in polar mesospheric clouds from SBUV version 3 PMC data. *Journal of Geophysical Research* 112, D10315.
- Fiedler, J., Baumgarten, G., von Cossart, G., 2005. Mean diurnal variations of noctilucent clouds during 7 years of lidar observations at ALOMAR. *Annales Geophysicae* 23, 1175–1181.
- Fritts, D.C., Isler, J.R., Thomas, G.E., 1993. Wave breaking signatures in noctilucent clouds. *Geophysical Research Letters* 20, 2039–2042.
- Gadsden, M., 1998. The north-west Europe data on noctilucent clouds: a survey. *Journal of Atmospheric and Solar-Terrestrial Physics* 60, 1163–1174.
- Gadsden, M., Schröder, W., 1989. *Noctilucent Clouds*. Springer, New York.
- Gardner, C.S., Miller, M.S., Liu, C.H., 1989. Rayleigh lidar observations of gravity wave activity in the upper stratosphere at Urbana, Illinois. *Journal of the Atmospheric Sciences* 46, 1838–1854.
- Gerrard, A.J., Kane, T.J., Thayer, J.P., 1998. Noctilucent clouds and wave dynamics: observations at Sondrestrom, Greenland. *Geophysical Research Letters* 25, 2817–2820.
- Gerrard, A.J., Kane, T.J., Thayer, J.P., Eckermann, S.D., 2004a. Concerning the upper stratospheric gravity wave and mesospheric cloud relationship over Sondrestrom, Greenland. *Journal of Atmospheric and Solar-Terrestrial Physics* 66, 229–240.
- Gerrard, A.J., Kane, T.J., Eckermann, S.D., Thayer, J.P., 2004b. Gravity waves and mesospheric clouds in the summer middle atmosphere: a comparison of lidar measurements and ray modeling of gravity waves over Sondrestrom, Greenland. *Journal of Geophysical Research* 109 (D10), D10103.
- Hecht, J.H., Thayer, J.P., Gutierrez, D.J., McKenzie, D.L., 1997. Multi-instrument zenith observations of noctilucent clouds over Greenland on July 30/31, 1995. *Journal of Geophysical Research* 102 (D2), 1959–1970.
- Hervig, M., Thompson, R.E., McHugh, M., Gordley, L.L., Russell III, J.M., Summers, M.E., 2001. First confirmation that water ice is the primary component of polar mesospheric clouds. *Geophysical Research Letters* 28, 971–974.
- Hostetler, C.A., Gardner, C.S., 1990. Rayleigh lidar signal processing techniques for studies of stratospheric temperature structure and dynamics, EOSL paper 90-003, University of Illinois at Urbana-Champaign.
- Jensen, E.J., Thomas, G.E., 1994. Numerical simulations of the effects of gravity waves on noctilucent clouds. *Journal of Geophysical Research* 99, 3421–3430.
- Merkel, A.W., Thomas, G.E., Palo, S.E., Bailey, S.M., 2003. Observations of the 5-day planetary wave in PMC measurements from the student nitric oxide explorer satellite. *Geophysical Research Letters* 30 (4), 1196.
- Portman, R.W., Thomas, G.E., Solomon, S., Garcia, R.R., 1995. The importance of dynamical feedbacks on doubled CO<sub>2</sub>-induced changes in the thermal structure of the mesosphere. *Geophysical Research Letters* 22, 1733–1736.
- Press, W.H., Flannery, B.P., Teukolsky, S.A., Vetterling, W.T., 1986. *Numerical Recipes: The Art of Scientific Computing*. Cambridge University Press, New York.

- Rapp, M., Thomas, G.E., 2006. Modeling the microphysics of mesospheric ice particles: assessment of current capabilities and basic sensitivities. *Journal of Atmospheric and Solar-Terrestrial Physics* 68, 71–744.
- Rapp, M., Lubken, F.-J., Mullemann, A., 2002. Small-scale temperature variations in the vicinity of NLC: experimental and model results. *Journal of Geophysical Research* 107 (D19), 4392.
- Senft, D.C., Gardner, C.S., 1991. Seasonal variability of gravity wave activity and spectra in the mesosphere region at Urbana. *Journal of Geophysical Research* 96, 17229–17264.
- Stevens, M.H., Meier, R.R., Chu, X., DeLand, M.T., Plane, J.M.C., 2005. Antarctic mesospheric clouds formed from space shuttle exhaust. *Geophysical Research Letters* 32, L13810.
- Swinbank, R., Ortland, D.A., 2003. Compilation of wind data for the upper atmosphere research satellite (UARS) reference atmosphere project. *Journal of Geophysical Research* 108 (D19), 4615.
- Thayer, J.P., Pan, W., 2006. Lidar observations of sodium density depletions in the presence of polar mesospheric clouds. *Journal of Atmospheric and Solar-Terrestrial Physics* 68, 85–92.
- Thayer, J.P., Rapp, M., Gerrard, A.J., Gudmundsson, E., Kane, T.J., 2003. Gravity wave influences on Arctic mesospheric clouds as determined by a Rayleigh lidar at Sondrestrom, Greenland. *Journal of Geophysical Research* 108 (D8), 8449.
- Thomas, G.E., 1991. Mesospheric clouds and the physics of the mesopause region. *Reviews of Geophysics* 29, 553–575.
- Thomas, G.E., 1996. Global change in the mesosphere–lower thermosphere region: has it already arrived? *Journal of Atmospheric and Solar-Terrestrial Physics* 58, 1629–1656.
- Thomas, G.E., Olivero, J.J., 2001. Noctilucent clouds as possible indicators of global change in the mesosphere. *Advances in Space Research* 28, 937–946.
- Thomas, G.E., Olivero, J.J., Jensen, E.J., Schroeder, W., Toon, O.B., 1989. Relation between increasing methane and the presence of ice clouds at the mesopause. *Nature* 338, 490–492.
- Turco, R.P., Toon, O.B., Whitten, R.C., Keesee, R.G., Hollenback, D., 1982. Noctilucent clouds: simulation studies of their genesis, properties, and global influences. *Planetary and Space Science* 30, 1147–1181.
- von Zahn, U., von Cossart, G., Fiedler, J., Rees, D., 1998. Tidal variations of noctilucent clouds measured at 69°N latitude by ground based lidar. *Geophysical Research Letters* 25, 1289–1292.
- Wilson, R., Chanin, M.L., Hauchecorne, A., 1991a. Gravity waves in the middle atmosphere observed by Rayleigh lidar 1. Case studies. *Journal of Geophysical Research* 96, 5153–5167.
- Wilson, R., Chanin, M.L., Hauchecorne, A., 1991b. Gravity waves in the middle atmosphere observed by Rayleigh lidar 2. Climatology. *Journal of Geophysical Research* 96, 5169–5183.
- Witt, G., 1962. Height, structure and displacements of noctilucent clouds. *Tellus* 14 (1), 1.
- Xu, J., Liu, H.-L., Yuan, W., Smith, A.K., Roble, R.G., Mertens, C.J., Russell III, J.M., Mlynczak, M.G., 2007. Mesopause structure from Thermosphere, Ionosphere, Mesosphere, Energetics, and Dynamics (TIMED)/Sounding of the Atmosphere Using Broadband Emission Radiometry (SABER) observations. *Journal of Geophysical Research* 112, D09102.
- Yamashita, C., Chu, X., Liu, H.-L., Espy, P.J., Nott, G.J., Huang, W., 2008. Stratospheric gravity wave characteristics and seasonal variations observed by lidar at the South Pole and Rothera, Antarctica. *Journal of Geophysical Research*, submitted for publication.